Iranian Journal of Science & Technology, Transaction B, Engineering, Vol. 32, No. B5, pp 471-490
Printed in The Islamic Republic of Iran, 2008

MODIFIED NON-STATIONARY CRITICAL INPUT EXCITATION BY A DESIGN ORIENTED OBJECTIVE FUNCTION*

P. ASHTARI[1] AND G. GHODRATI AMIRI[2**]

[1]College of Civil Engineering, Iran University of Science & Technology, Tehran, I. R. of Iran
[2]Center of Excellence for Fundamental Studies in Structural Engineering, Iran University of Science & Technology, Tehran, I. R. of Iran, Email: ghodrati@iust.ac.ir

Abstract– Nowadays, seismic design of structures performed by any seismic code is based on resisting previous natural earthquakes. Therefore, the critical excitation method has been proposed in recent years to consider probable future earthquakes that may be more destructive. Non-stationary critical excitation for a structure is found under specified constraints to resonate the structure. In this paper, the objective function of non-stationary critical excitation is taken as the maximization of all the inter-storey drifts at different times, separately. The power (area under power spectral density function) and the intensity (magnitude of PSD function) are limited, and critical excitation is found according to these constraints. Three techniques of finding non-stationary critical excitation are proposed, *optimum line*, *simple* and *modified* techniques. Then, the proposed techniques are used in many MDOF models and the results are investigated.

Keywords– Critical excitation, non-stationary input, optimization, random vibration, design

1. INTRODUCTION

Earthquake is an uncertain and unpredictable phenomena and it is always possible for a more destructive earthquake to occur in the future. Therefore, seismic design of structures based only on withstanding previous earthquakes seems to be inadequate. However, static and modal seismic designs of structures are based on the design spectrum produced by previous earthquakes. In addition, time-history analysis of structures applies previous accelerograms.

For the first time, A. Papoulis [1] introduced the critical excitation concept in electrical engineering in 1967. Then, R.F. Drenick [2] used the method of critical excitation for structures in time domain. In this method, an input excitation is obtained which produces the maximum response from a class of allowable inputs. In addition, M. Shinozuka [3] expressed the same method in the frequency domain and presented a narrower upper bound of the maximum response.

Critical excitation method is an optimization problem to be solved having an objective function and constraints. Until now, many people have worked on different constraints and objective functions. Iyengar, Manohar, Sarkar and Takewaki are researchers who extended the method to a stochastic problem to consider the uncertain characteristics of an earthquake [4-9]. Also, Ben-Haim, Elishakoff, Pantelides and Tzan presented several interesting convex models [10, 11]. Critical excitation method produces artificial earthquakes that have greater responses than other artificial record generation methods using wavelet theory [12] and random and geophysics models [13].

Recently, Takewaki [8] has developed a new optimization problem in frequency domain for finding non-stationary input excitation. His proposed constraints were the power limit (area under power spectral density (PSD) function) and the intensity limit (magnitude of PSD function). Solving this nonlinear

*Received by the editors January 31, 2007; Accepted December 2, 2007.
**Corresponding author

optimization problem is complicated and time-consuming for non-stationary input excitation considering response resonance of higher modes of structure with input excitation.

Ashtari [14] introduced "Optimum Line" as a geometric technique of solving the stationary optimization problem. Then, an exact method for SDOF systems and a simple numerical technique were presented [15] to find stationary critical excitation for MDOF systems. Finally, a modified technique was proposed [16] that could reduce the time and steps of the solution to produce more exact responses. In the previous methods, input excitation was supposed to be stationary, but earthquake is a non-stationary random excitation. In the present paper, the modified technique presented earlier by these authors is extended and the input is taken as non-stationary excitation. In addition, a design oriented objective function is proposed for a critical excitation optimization problem. Finally, this technique is applied to many SDOF and MDOF models and the resultant conclusions are presented.

2. INTRODUCING CRITICAL EXCITATION OPTIMIZATION PROBLEM

Input excitation can be a stationary or non-stationary process. First, an introduction to the random vibration theory is expressed to find the mean square of all inter-storey drifts as the objective function. Next, the proposed optimization problem for finding non-stationary critical excitation is presented.

According to Bendat and Piersol's model [17], input horizontal ground acceleration $\ddot{u}_g$ is expressed by

$$\ddot{u}_g(t) = c(t)w(t) \tag{1}$$

where $c(t)$ is a deterministic envelope function and $w(t)$ is a zero mean stationary Gaussian process. The equation of motion for the MDOF system can be expressed by [18]

$$\boldsymbol{M}\ddot{\boldsymbol{u}}(t) + \boldsymbol{C}\dot{\boldsymbol{u}}(t) + \boldsymbol{K}\boldsymbol{u}(t) = -\boldsymbol{M}\boldsymbol{r}\,\ddot{u}_g(t) \tag{2}$$

$\boldsymbol{M}$, $\boldsymbol{C}$ and $\boldsymbol{K}$ represent the system mass, viscous damping and stiffness matrices respectively, and $\boldsymbol{r} = \{1, \ldots, 1\}^t$ represents the influence coefficient vector for transferring displacements to drifts. The displacement vector $\boldsymbol{u}(t)$ can be expanded in terms of modal coordinates $\boldsymbol{q}(t) = \{q_j\}$.

$$\boldsymbol{u}(t) = \boldsymbol{\Phi}\boldsymbol{q}(t) \tag{3}$$

Because of the orthogonality condition of natural modes, substitution of the mentioned coordinate transformation into the equation of motion (2) for the MDOF system leads to the uncoupled equations for the shear building model as shown in Fig. 1 [18 and 19].

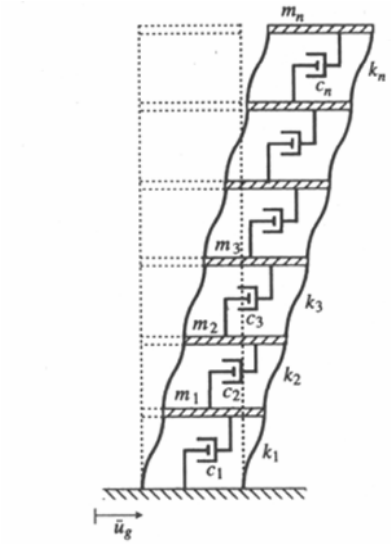

Fig. 1. n-story shear building model subjected to horizontal base acceleration [8]

$$\ddot{q}_j + 2\xi_j \omega_j \dot{q}_j + \omega_j^2 q_j = -\Gamma_j \ddot{u}_g(t) \quad : (j = 1,...,n) \tag{4}$$

Where the j^{th} mode participation factor (Γ_j) for the shear building model is computed by

$$\Gamma_j = \frac{\sum_{i=1}^{n} m_i \phi_i^{(j)}}{\sum_{i=1}^{n} m_i \phi_i^{(j)^2}} \tag{5}$$

So the mean square of the k^{th} inter-storey drift can be calculated by

$$\sigma_{d_k}(t)^2 = \int_{-\infty}^{+\infty} H_M(k,t;\omega)\, S_w(\omega)\, d\omega \tag{6}$$

where $H_M(k,t;\omega)$, generally called F-function, *is [8]*

$$F(k,t;\omega)=H_M(k,t;\omega)=[\sum_{j=1}^{n} \Gamma_j (\varphi_k^{(j)} - \varphi_{k-1}^{(j)})\, A_{Cj}(t\,;\omega)]^2 + [\sum_{j=1}^{n} \Gamma_j (\varphi_k^{(j)} - \varphi_{k-1}^{(j)})\, A_{Sj}(t\,;\omega)]^2 \tag{7}$$

Where,

$$A_{Cj}(t\,;\omega) = \int_0^t c(\tau)\, g_j(t-\tau)\, \cos\omega\tau\, d\tau \tag{8}$$

$$A_{Sj}(t\,;\omega) = \int_0^t c(\tau)\, g_j(t-\tau)\, \sin\omega\tau\, d\tau \tag{9}$$

In which the function $g_j(t) = H_e(t)\ (1/\omega_{jd})\, e^{-\xi\omega_j t} \sin(\omega_{jd}\, t)$ is the unit impulse response function ($H_e(t)$: Heaviside step function, $\omega_{jd} = \sqrt{1-\xi^2}\,\omega_j$).

Therefore, the optimization problem of finding non-stationary critical excitation can be expressed as

$$\underset{S_w(\omega)}{Max}\ \underset{k}{Max}\ \underset{t}{Max}\ \sigma_{d_k}^2(t) = \int_{-\infty}^{+\infty} H_M(k,t;\omega)\, S_w(\omega)\, d\omega \tag{10}$$

Subjected to

$$\int_{-\infty}^{+\infty} S_w(\omega)\, d\omega \le \bar{S}_w \qquad (\bar{S}_w = \text{Given power limit}) \tag{11}$$

$$\sup\ S_w(\omega) \le \bar{s}_w \qquad (\bar{s}_w = \text{Given PSD amplitude limit}) \tag{12}$$

This optimization problem consists of a triple maximization procedure. According to this optimization problem, an input spectrum, $S_w(\omega)$, is found in which the mean square of one of the inter-storey drifts at a time reaches its maximum value under two constraints. The input PSD is called critical PSD. Takewaki [8, 9] used the sum of the mean squares of the inter-storey drifts as the objective function. However, it is known that sometimes the inter-storey drift of a specific story, for example soft story, can be much more than that of other storeys and can cause the complete collapse of the structure, although the sum of the inter-storey drifts can be at an allowable range.

If the heights of the stories are different, it is better to maximize the ratio of the inter-storey drift to the story height as the objective function.

$$\underset{S_w(\omega)}{Max}\ \underset{k}{Max}\ \underset{t}{Max}\ \frac{\sigma_{d_k}^2}{h_k^2} \tag{13}$$

This will guide us to displacement-based design trend. In this paper, because of unknown story heights, we assume that the heights of stories are equal. Therefore, Eq. (10) is selected as the objective function.

3. PROPOSED TECHNIQUE FOR FINDING OPTIMAL NON-STATIONARY CRITICAL EXCITATION FOR MULTI-STORY BUILDINGS

Because the proposed technique is based on the integration of the F-function, the different shapes of the F-function are explained first. Then, the proposed technique will be presented.

a) Shape of the F-function F(k,t ;ω)

As seen in the previous section, the objective function of critical excitation optimization is to maximize the integration of the multiplication of two functions: *F-function and* $S_w(\omega)$. According to the maximization, the peaks of F-function participate in the critical excitation. Therefore, in MDOF systems, F-function peaks become important from two viewpoints: the number of the peaks and the height of the peaks.

$F(\omega)$ is a function of dynamic parameters of the structure like modal frequencies and damping. In MDOF systems, the number of principle peaks is less than or equal to the dynamical degree of freedom of the structure. In Fig. 2, three models with different modal frequencies are demonstrated (mass in kg and stiffness in N/m). In Figs. 3, 4 and 5, the F-functions of the 2-DOF models of Fig. 2 are shown for non-stationary input.

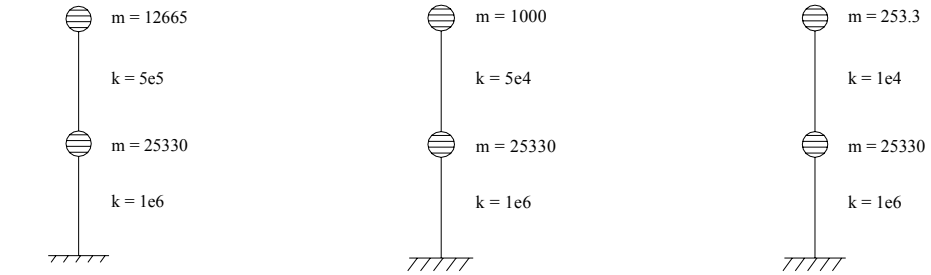

Model 1 Model 2 Model 3

Fig. 2. Three 2-DOF systems

Fig. 3 shows distant peaks for Model 1. In Fig. 4, the effect of near modal frequencies is illustrated and in Fig. 5, two peaks are combined and reduced to one peak. Fig. 6 illustrates the F-function of a six-story building. As seen in these figures, the first peak of the F-function relative to the first mode is the highest peak and the height of the peaks of the higher modes gradually decreases. This height decrease is approximately linear in a semi-logarithmic curve.

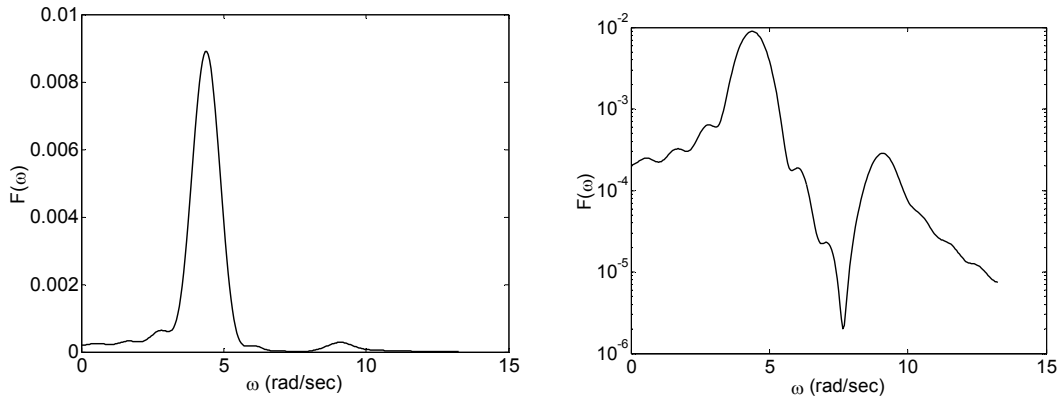

(a) (b)

Fig. 3. F-function of non-stationary critical excitation for 2-DOF Model 1

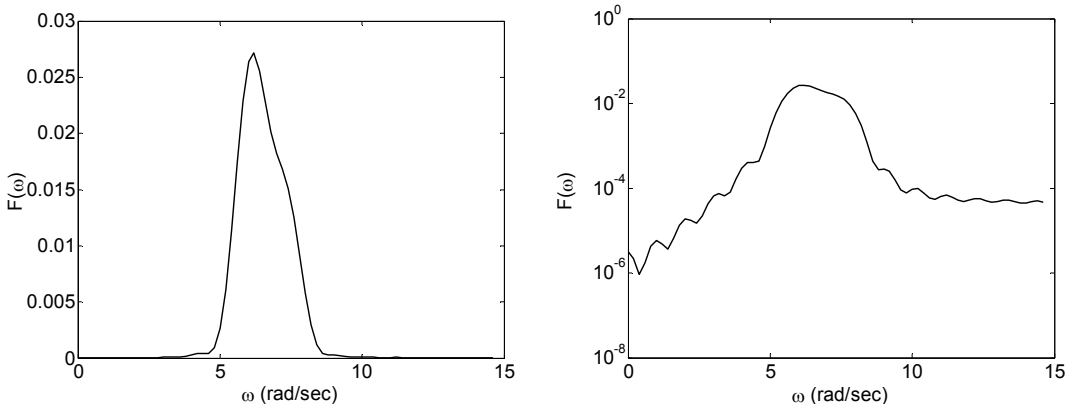

(a) (b)

Fig. 4. F-function of non-stationary critical excitation for 2-DOF Model 2

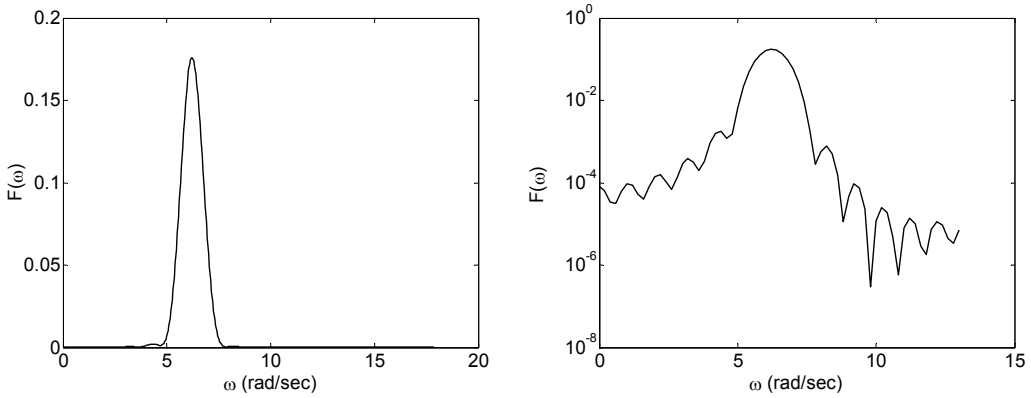

(a) (b)

Fig. 5. F-function of non-stationary critical excitation for 2-DOF Model 3

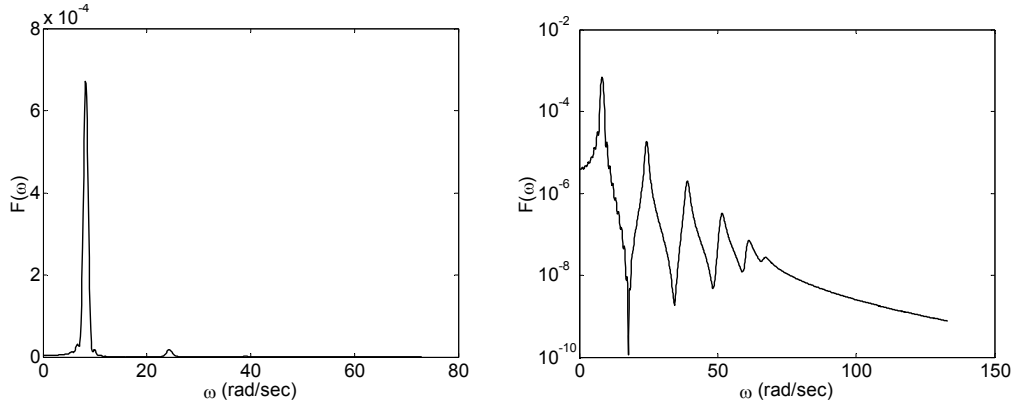

(a) (b)

Fig. 6. F-function of non-stationary critical excitation for a six-story building

As previously mentioned, the peaks of F-function are higher in the first modes and become lower in the higher modes. As a generalization for 2-DOF systems, a frequency range ($\Delta\hat{\omega}$) around the first mode can be found in which F-function values are higher than the peak value of the second mode. In Fig. 7, this frequency range is shown between $\hat{\omega}_1$ and $\hat{\omega}_2$.

The critical excitation frequency bandwidth can be calculated according to the constraints of the optimization problem. If this calculated bandwidth is narrower than $\Delta\hat{\omega}$, only the first peak will participate in the frequency content of critical excitation because of greater F-function values. However, for the wider frequency bandwidth, the second peak related to the second mode will contribute [14].

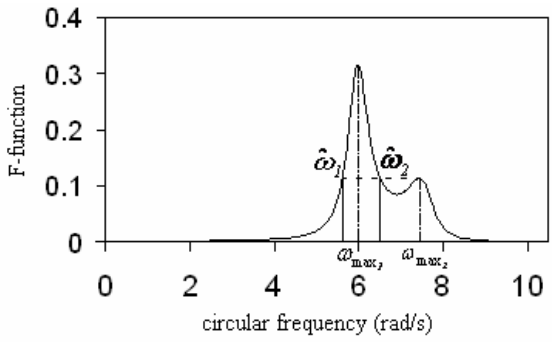

Fig. 7. Higher range of the first mode

b) Proposed technique

The first step of the algorithm is to exchange the order of maximization procedure [8]. Therefore, the objective function of Eq. (10) converts to

$$\underset{k}{Max}\ \underset{t}{Max}\ \underset{S_w(\omega)}{Max}\ \left\{f(k,t,S_w)=\sigma_{d_k}^2(t)\right\} \tag{14}$$

According to this maximization, for every story k at different times, a function $S_w^{\max}(\omega)$ is found to maximize f.

$$f_{\max}(m,n)=f(k_m,t_n,S_w^{\max}(\omega)) \tag{15}$$

Where

$$f(k_m,t_n,S_w^{\max}(\omega))=\underset{S_w(\omega)}{Max}\ f(k_m,t_n,S_w(\omega)) \tag{16}$$

Then, the maximum values of f at different times are compared together and the time that has the greater value of f is calculated (f *at* t_{max}). Finally, the greatest value between the maximum f values of all the stories ($f_{\max}$) is computed as the response of the non-stationary critical excitation optimization problem.

$$\underset{k_m}{Max}\ \underset{t_n}{Max}\ \underset{S_w(\omega)}{Max}\ f(k_m,t_n,S_w)=f(k_m,t_n,S_w^{\max})\ :k_m=k_{\max}\ ,t_n=t_{\max} \tag{17}$$

In other words, there is a matrix $[f_{\max}]_{m\times n}$ with components of $f_{max}(m,n)$ at different stories k_m, and times t_n.

$$[f_{\max}(m,n)]=[f(k_m,t_n,S_w^{\max}(\omega))] \tag{18}$$

Therefore, the final answer of the optimization problem is the greatest component of $[f_{\max}]_{m\times n}$.

$$Max\ [f_{\max}(m,n)]=f(k_{\max},t_{\max},S_w^{\max}(\omega)) \tag{19}$$

This means that the maximum mean square of inter-storey drift can take place at story k_{max} and time t_{max}.
In the next two sections, two techniques of finding $S_w^{\max}(\omega)$ are proposed.

1- Simple technique for non-stationary critical excitation: The main part of the solution of the proposed optimization problem is to find the power spectral density of $w(t)$, called $S_w(\omega)$, to maximize f-function in the specified story k and time t. It is taken as

$$F_{m,n}(\omega)=H_M(k_m\ ,\ t_n\ ;\ \omega) \tag{20}$$

Therefore, Eq. (6) reduces to the following form

$$\sigma_{d_{k_m}}(t_n)^2 = \int_{-\infty}^{+\infty} F_{m,n}(\omega) S_w(\omega)\, d\omega \tag{21}$$

Since *w(t)* is a stationary Gaussian process, the non-stationary optimization problem at a specified time and story becomes similar to the stationary critical excitation problem [8, 14-16]. To maximize this integration, it is evident that $S_w(\omega)$ should be equal to its extreme value $\bar{s}_w$ in the frequency ranges. Therefore,

$$\sigma_{d_{k_m}}(t_n)^2 = \bar{S}_w \int_{-\infty}^{+\infty} F_{m,n}(\omega)\, d\omega \tag{22}$$

Now, the frequency bands ($\Delta\omega_1$,$\Delta\omega_2$,$\cdots$) should be calculated. Fig. 8 shows these rectangular frequency bands having positions critical to the excitation solution. As seen in Fig. 9, the intersections of F-function with these rectangular frequency bands are placed on a straight line called "Optimum Line". For a fixed total frequency bandwidth ($\Delta\omega_{total}$), if the position of each of the frequency bands is changed, F-function will experience fewer values. This shows the importance of "Optimum Line" as a geometric solution of "critical excitation "optimization problem [14].

$$\Delta\omega_{total} = \Delta\omega_1 + \Delta\omega_2 + \ldots = \frac{\bar{S}_w}{\bar{s}_w} \tag{23}$$

Although, the "Optimum Line" technique is conceptual and meaningful, but it is difficult to find the position of the "Optimum Line" and its intersections with F-function. Therefore, it will be necessary to present a simple numerical technique [15].

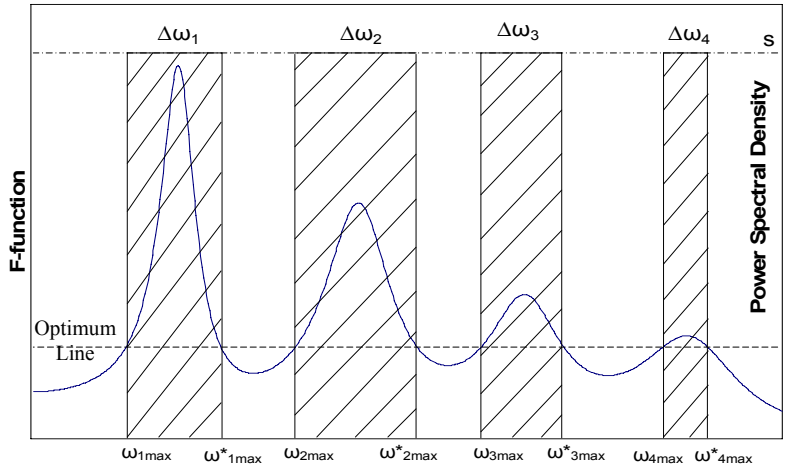

Fig. 8. Schematic position of frequency bands of modes [14]

To find the frequency bands, a probable frequency range (ω_0, ω_c) is chosen and is divided into $\delta\omega$ s. The middle point of each $\delta\omega$ is found, then $F_{m,n}(\omega)$ for all the start, the end and the middle points are calculated. So the area under $F_{m,n}(\omega)$ in each $\delta\omega$ can be computed using the quadratic approximation of the Simpson method of integration.

$$\delta A_i^{m,n} = \int_{\omega_1=\omega_1^i}^{\omega_2=\omega_1^i+\delta\omega} F_{m,n}(\omega)\; d\omega = \frac{\delta\omega}{6}\left[F_{m,n}\left(\omega_1^i\right) + 4F_{m,n}\left(\omega_1^i + \frac{\delta\omega}{2}\right) + F_{m,n}\left(\omega_1^i + \delta\omega\right)\right] \tag{24}$$

After finding the δA_i s for all the $\delta\omega_i$ s, they are sorted in descending order

$$\delta A_1^{m,n} \geq \delta A_2^{m,n} \geq \delta A_3^{m,n} \geq \ldots \tag{25}$$

Now, according to the linear interpolation, it approximately becomes

$$Max \int F_{m,n}(\omega)\, d\omega = \sum_{i=1}^{[N]} \delta A_i^{m,n} + (N - [N])\ \delta A_{[N]+1}^{m,n} \tag{26}$$

Where $[N]$ is the round part of $N = \frac{\overline{S}/\overline{s}}{\delta\omega}$. By decreasing $\delta\omega$ s, δA s decrease and the Eq. (26) can be approximately reduced to the simplified form [15]

$$Max \int F_{m,n}(\omega)\, d\omega = \sum_{i=1}^{[N]} \delta A_i^{m,n} \tag{27}$$

Therefore, while using small steps, the answer of the optimization problem at a specific time and story becomes

$$\underset{S_w(\omega)}{Max}\ f(k_m, t_n, S_w^{\max}) = \underset{S_w(\omega)}{Max}\ \sigma_{d_{k_m}}^2(t_n) = \overline{s}_w \sum_{i=1}^{[N]} \delta A_i^{m,n} \tag{28}$$

2. Modified technique for non-stationary critical excitation

Simple technique is based on interval rectangles for calculating the area under the F-function. Therefore, the simple technique requires so many steps to achieve a specified accuracy and is inefficient, especially for large structures. To overcome this disadvantage, the modified technique is presented. In Fig. 10, a peak of F-function has been illustrated. It is seen that in the simple technique, ω_1 *and* ω_2 do not have equal $F(\omega)$.

As introduced in [14], "Optimum Line" is the exact geometric solution. So the exact frequency range of the peak of F-function is the intersection of "Optimum Line" with F-function curve.

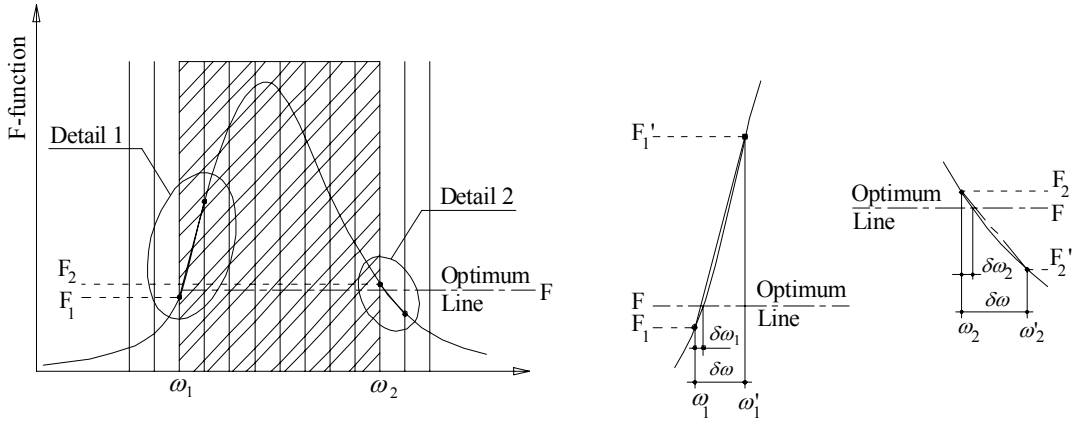

(a) (b) Detail 1 (c) Detail 2

Fig. 9. Modified optimization technique [16]

In Fig. 9, the i^{th} peak of F-function is given as

$$F = F_{m,n}(\omega) = H_M(k_m, t_n;\ \omega) \tag{29}$$

$$F_1^i = F_{m,n}^i(\omega_1) = H_M^i(k_m, t_n;\ \omega_1) \tag{30}$$

$$F_2^i = F_{m,n}^i(\omega_2) = H_M^i(k_m, t_n;\ \omega_2) \tag{31}$$

To equalize F-functions of the start and the end frequencies of the bandwidths and to produce an "Optimum Line" as shown in Fig. 9(a), the start and the end frequencies (ω_1 *and* ω_2) should be modified. By assuming the F-function will change linearly in each step $\delta\omega$, it is found from Figs. 9 (b, c)

$$F = F_1^i + m_1^i \delta\omega_1^i \qquad \text{(Detail 1)} \tag{32}$$

$$F = F_2^i + m_2^i \delta\omega_2^i \qquad \text{(Detail 2)} \tag{33}$$

therefore

$$F_1^i + m_1^i \delta\omega_1^i = F_2^i + m_2^i \delta\omega_2^i = \ldots \tag{34}$$

In addition, to include the decimal part, it is

$$\sum^{i} (-\delta\omega_1^i + \delta\omega_2^i) = \delta\omega_r \tag{35}$$

where

$$\delta\omega_r = \left(\overline{S}_w / \overline{s}_w\right) - \left[\frac{\overline{S}_w / \overline{s}_w}{\delta\omega}\right]\delta\omega \tag{36}$$

For $S_w(\omega)$ having only one rectangle, combining two Eqs. (34) and (36) results in

$$\delta\omega_1 = -\frac{\Delta F}{\Delta m} + \frac{m_2}{m_1 - m_2}\delta\omega_r \tag{37}$$

$$\delta\omega_2 = -\frac{\Delta F}{\Delta m} + \frac{m_1}{m_1 - m_2}\delta\omega_r \tag{38}$$

If $\delta\omega_r$ is close to zero,

$$\delta\omega_1 = \delta\omega_2 = -\frac{\Delta F}{\Delta m} \tag{39}$$

For MDOF systems where critical input excitation becomes two or more rectangles, the general formula becomes

$$\delta\omega_1 = \frac{\sum_{i=2}^{2n} \frac{F_i - F_1}{|m_i|} - \delta\omega_r}{1 + m_1 \sum_{i=2}^{2n} \frac{1}{|m_i|}} \tag{40}$$

In which, F_i *and* m_i are the F-function value and the slope of the i^{th} intersection of "Optimum Line" with F-function, respectively. n is the number of frequency rectangles of critical input excitations. Also, other $\delta\omega_i$ s can be calculated

$$\delta\omega_i = \frac{1}{m_i}\left(F_1 - F_i + m_1\delta\omega_1\right) \qquad : i = 2\ ,\ \ldots\ ,\ 2n \tag{41}$$

$\delta\omega_i$ s could be positive or negative. Therefore, there is this general equation

$$\omega_i^{\text{modified}} = \omega_i^{simple} + \delta\omega_i \ : i=2\ ,\ \ldots\ ,\ 2n \tag{42}$$

If the first frequency bandwidth rectangle starts from zero frequency, it will be $\delta\omega_1 = 0$ and

$$\delta\omega_2 = \frac{\sum_{i=3}^{2n} \frac{F_2 - F_i}{|m_i|} + \delta\omega_r}{1 - m_2 \sum_{i=3}^{2n} \frac{1}{|m_i|}} \tag{43}$$

In the same way, $\delta\omega_i$ s and $\omega_i^{\mathrm{mod}ified}$ s will be computed by Eqs. (41) and (42) for ($i=3,...,2n$). So the modified area of F-function is calculated.

$$Modified\ \ Area = \sum_{i=1}^{[N]} \delta A_i^{m,n} + \sum^{i} \left\{ - \int_{\omega_1^i}^{\omega_1^i + \delta\omega_1^i} F_{m,n}(\omega)\ d\omega + \int_{\omega_2^i - \delta\omega_2^i}^{\omega_2^i} F_{m,n}(\omega)\ d\omega \right\} \tag{44}$$

Two integrations in the above formula are taken by the Simpson method. So

$$\underset{S_w(\omega)}{Max}\ \ f(k_m, t_n, S_w^{\max}) = \underset{S_w(\omega)}{Max}\ \ \sigma_{d_{k_m}}^2(t_n) = \bar{s}_w \times Modified\ \ Area \tag{45}$$

4. NUMERICAL EXAMPLES

A MATLAB computer program has been prepared to apply the algorithm of the proposed technique. This program accepts inputs by defining new parameters or selecting default values. Output is presented as a word file and a collection of figures. In this section, the following envelope function will be used

$$c(t) = e^{-\alpha t} - e^{-\beta t} \tag{46}$$

The parameters $\alpha=0.115$ and $\beta=0.465$ are selected to have an earthquake duration of *30 s* and a peak at *4 s*.

1. SDOF model: Consider a SDOF system having a mass and stiffness of 25330 kg and 1×10^6 N/m, respectively. Therefore, the period of the model becomes equal to one second. A damping ratio of 0.05 is assumed. If the period of non-stationary input excitation is around one second, resonance will increase the responses. Fig. 10 illustrates sub-figures related to SDOF critical excitation under El-Centro earthquake (NS 1940) power and magnitude limit. In other words, $\bar{S}_w$ and $\bar{s}_w$ are equal to 1.23 and 1.00, respectively. In Fig. 10a, three-dimensional curves of F-function are plotted at various times and frequencies. At any distinct time, F-function has a peak around $\omega = 6.28$ rad/s. When the height of the peak increases, the bandwidth of the peak becomes narrower. The highest peak occurs at $t=8$ s. In Fig. 10b, the value of $\sigma_d{}^2(t)$ is plotted at different times. It can be observed that at $t=7$ s, the drift value reaches its maximum value. Therefore, Fig. 10d shows F-function values at $t_{max}=7$ s as semi-logarithmic plot. For an SDOF model, plotting $\sigma_d{}^2(t_{\max})$ against different stories gives only one point. In Fig. 10e, non-stationary critical input excitation is found by using the proposed technique. This figure shows that the middle point of the hatched frequency bandwidth is placed around the natural frequency.

a) Two degrees of freedom models

Three 2-DOF models have been investigated, *Model 1, Model 2 and Model 3*. The floor masses and story stiffnesses of these models are as shown in Fig. 2. A damping ratio of 0.05 is selected for all the models.

1. Model 1: Frequencies of the first and the second modes are 4.44 and 8.88 rad/s that are adequately far from each other (Fig. 11c). In Fig. 11, power and magnitude constraints are taken from the El-Centro (NS 1940) earthquake. Fig. 11a shows three-dimensional curves of F-function at different times and frequencies. At each time, F-function has two peaks. As seen, these peaks, at the first seconds of the earthquake, are wider and lower. Gradually, the peaks become higher and narrower. At $t=8$ s, two peaks of F-function are the highest and the narrowest. Again, after this time, the height of the peaks decreases. In Fig. 12b, $\sigma_{d_k}^2$ for critical (first) story during time is plotted. It can be observed that inter-storey drift of the critical story becomes maximum value at *t=7 s*. Fig. 11c illustrates the F-function at t_{max} *and* k_{max}. In Fig. 11 d, inter-story drifts of the first and the second stories are compared. Therefore, the results show that the first story is critical and has a greater mean square of inter-story drift. Fig. 11e shows the critical input

excitation bandwidth obtained by the proposed modified technique. As can be observed, critical input frequency is only one rectangular bandwidth around the peak of the first mode because of assuming narrowband input frequency.

In Fig. 12, non-stationary critical excitation is found for an assumed earthquake having wider input frequency bandwidth. $\overline{S}_w$ and $\overline{s}_w$ are equal to 4.43 and 1.00, respectively. As seen, the mean square of the inter-storey drift of the second story reaches its maximum value at *t=7 s*. This means that maximum response does not occur in the highest peak at *t=8 s*. The other important point in this example is that critical input excitation has two frequency bandwidths around the frequencies of the first and the second modes (Fig. 12e).

In Fig. 13, non-stationary critical excitation is computed for the power and magnitude limit of the Tabas earthquake (1978), having a very wide input frequency range. $\overline{S}_w$ and $\overline{s}_w$ are equal to 7.63 and 1.00, respectively. Here, the second story, at *t=6 s*, has maximum mean square of inter-story drift. As seen in Fig. 13e, the critical input excitation becomes one wide rectangular frequency bandwidth covering the frequencies of the peaks at the first and the second modes.

2. Model 2: The circular frequency of the first and the second modes of the model are equal to 5.9 and 7.5 rad/s, respectively that are close together. In Fig. 14, non-stationary critical input excitation is shown by assuming the optimization limits from the El-Centro (NS 1940) earthquake. Fig. 14a illustrates F-function at different times and frequencies. In the first seconds of earthquake occurrence, F-function peaks are wider and lower. In addition, F-function has only one peak. After *t=7 s*, peaks become higher and two peaks of two modal frequencies are revealed. As seen in Figs. 14b and 14d, the second story, at *t=7 s,* has the greatest mean square of inter-story drift. Because of narrowband input constraint (El-Centro), critical input excitation is restricted to the first peak. In spite of our expectation from critical excitation (Fig. 14e), F-function at the second peak is higher than F-function of the edges of the critical excitation frequency bandwidth. In this case, $\delta\omega$ should be changed to smaller values to increase the accuracy. Previously, $\delta\omega$ was equal to 0.2. Now, we assume $\delta\omega = 0.04$, critical excitation is computed (Fig. 15), and critical input excitation changes from one frequency bandwidth to two rectangular frequency bandwidths. Fig. 16 illustrates the critical excitation for the Tabas earthquake (1978). Comparing Fig. 11 to Fig. 15 shows that, when the input frequency bandwidth becomes wider, critical input excitation relates to the earlier times of earthquake duration.

In Table 1, critical excitation has been found for three frequency steps equal to *0.5, 0.2 and 0.01 rad/s*. It is known that when the frequency step becomes larger, the program running time decreases because of less mathematical computation. For example, if the frequency step ($\delta\omega$) is enlarged 2.5 times to increase $\delta\omega$ from 0.2 to 0.5 rad/sec, the program running time approximately decreases to 40 % of the initial time. In addition, according to Table 1, if $\delta\omega$ =0.5 is used in the modified technique, the error will become 0.3 %, which is less than the error of simple technique using $\delta\omega$ =0.2 equal to 0.5 %. Therefore, it results in the modified technique decreasing the program running time to half and even less, for a fixed error.

3. Model 3: The frequency of the first and the second modes are equal to 9.5 and 10.5 rad/s, respectively. They are so much closer to each other. In Fig. 17, critical input excitation is shown by assuming the optimization constraints from the El-Centro (1978) earthquake. Fig. 17 illustrates F-function having only one peak. In other words, two frequencies of the model are so close together that it causes two peaks to be combined into one peak.

b) Four and six story buildings

In Fig. 18, critical excitation is found for a four-story building with floor masses and story stiffnesses as 1×10^4 kg and 1×10^6 N/m, respectively. The limits are the power and extreme magnitude of the Tabas

earthquake (1978). The first bandwidth starts from zero frequency and the second bandwidth is placed at a small peak because of non-stationary input. Fig. 19 shows critical excitation curves for a six-story building. Its floor mass and story stiffness are 3.2×10^4 kg and 3.76×10^7 N/m, respectively. The constraints are taken from the Hyogoken-Nanbu, JMA Kobe NS 1995 earthquake. Input frequency gathers around the first and the second modes.

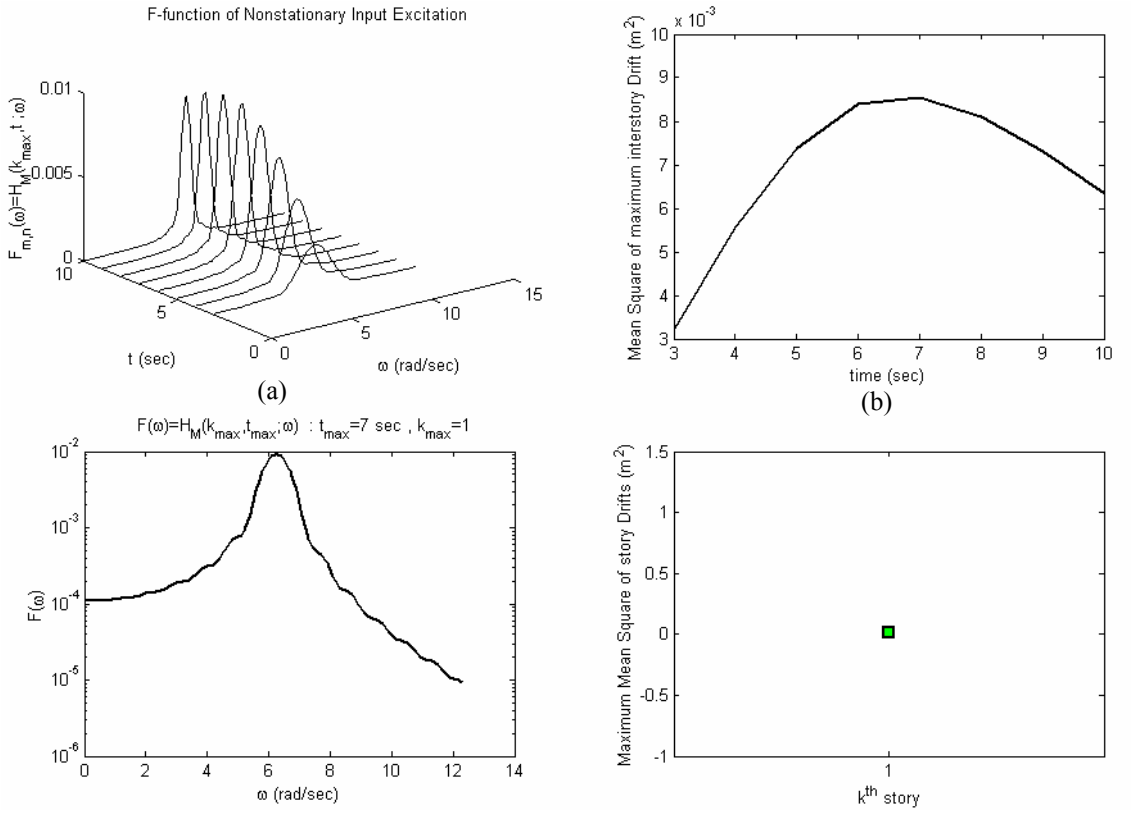

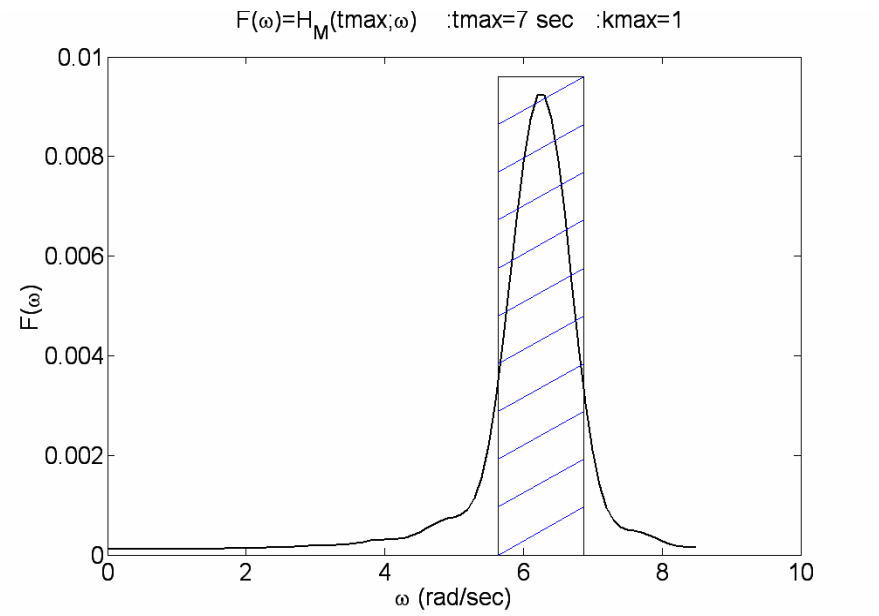

Fig. 10. Non-stationary critical excitation for SDOF model under El-Centro constraints (NS 1940)

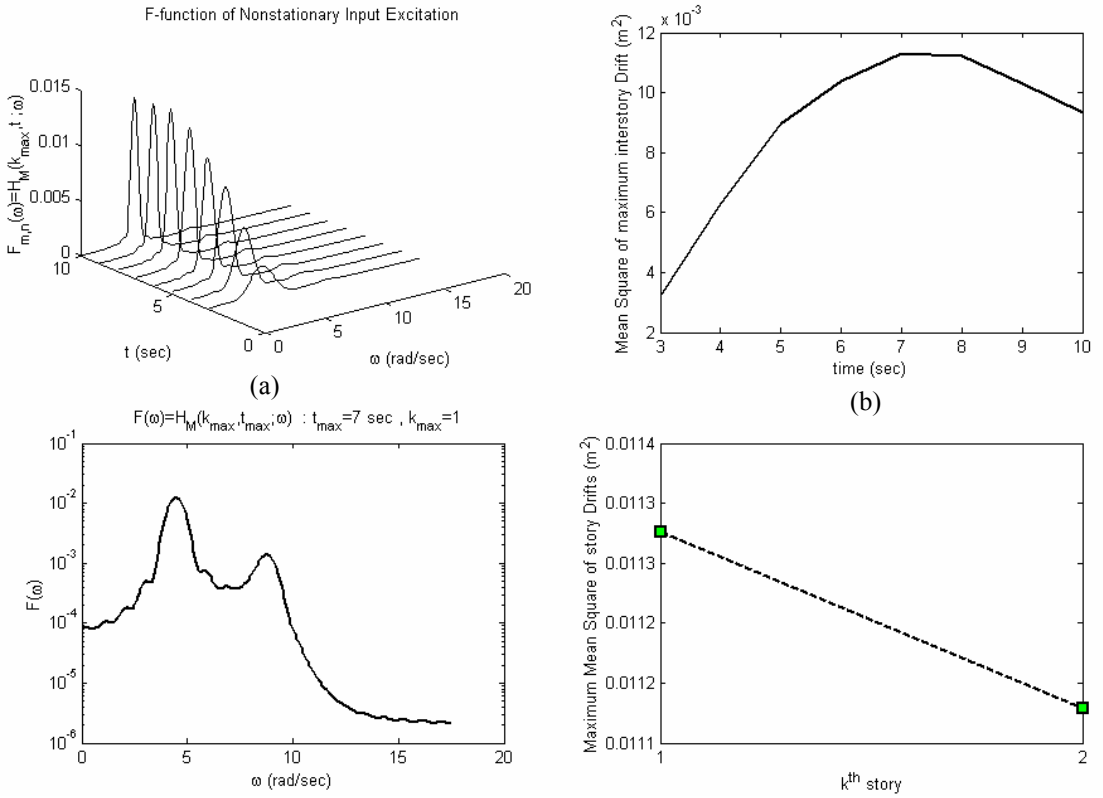

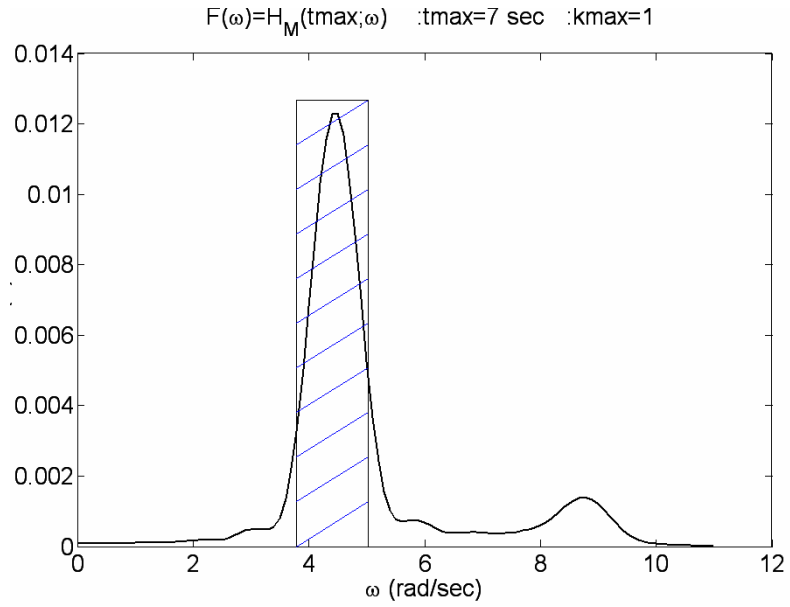

(e)

Fig. 11. Non-stationary critical excitation for Model 1 under El-Centro constraints (NS 1940)

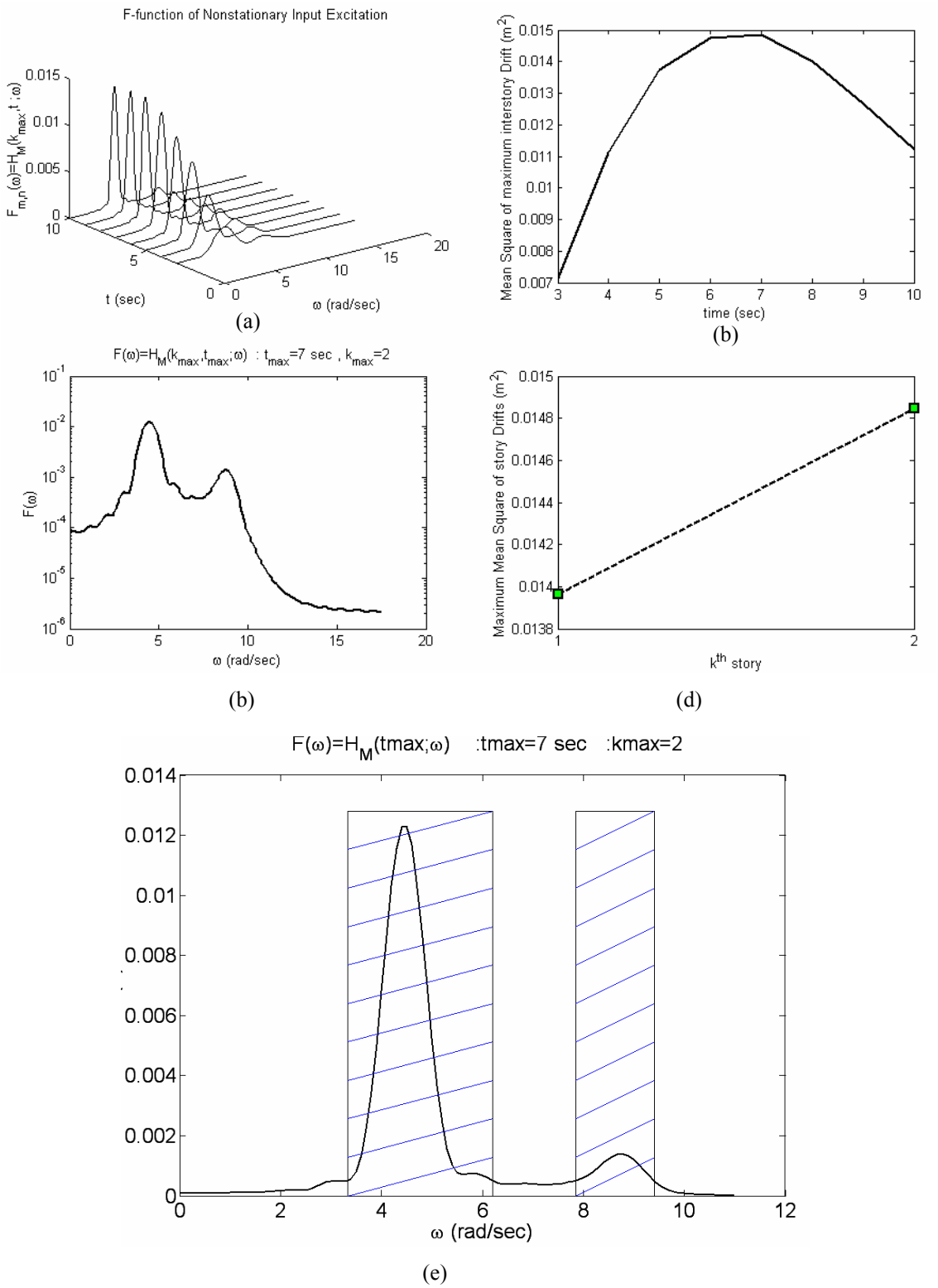

Fig. 12. Non-stationary critical excitation for Model 1 under the assumed constraints

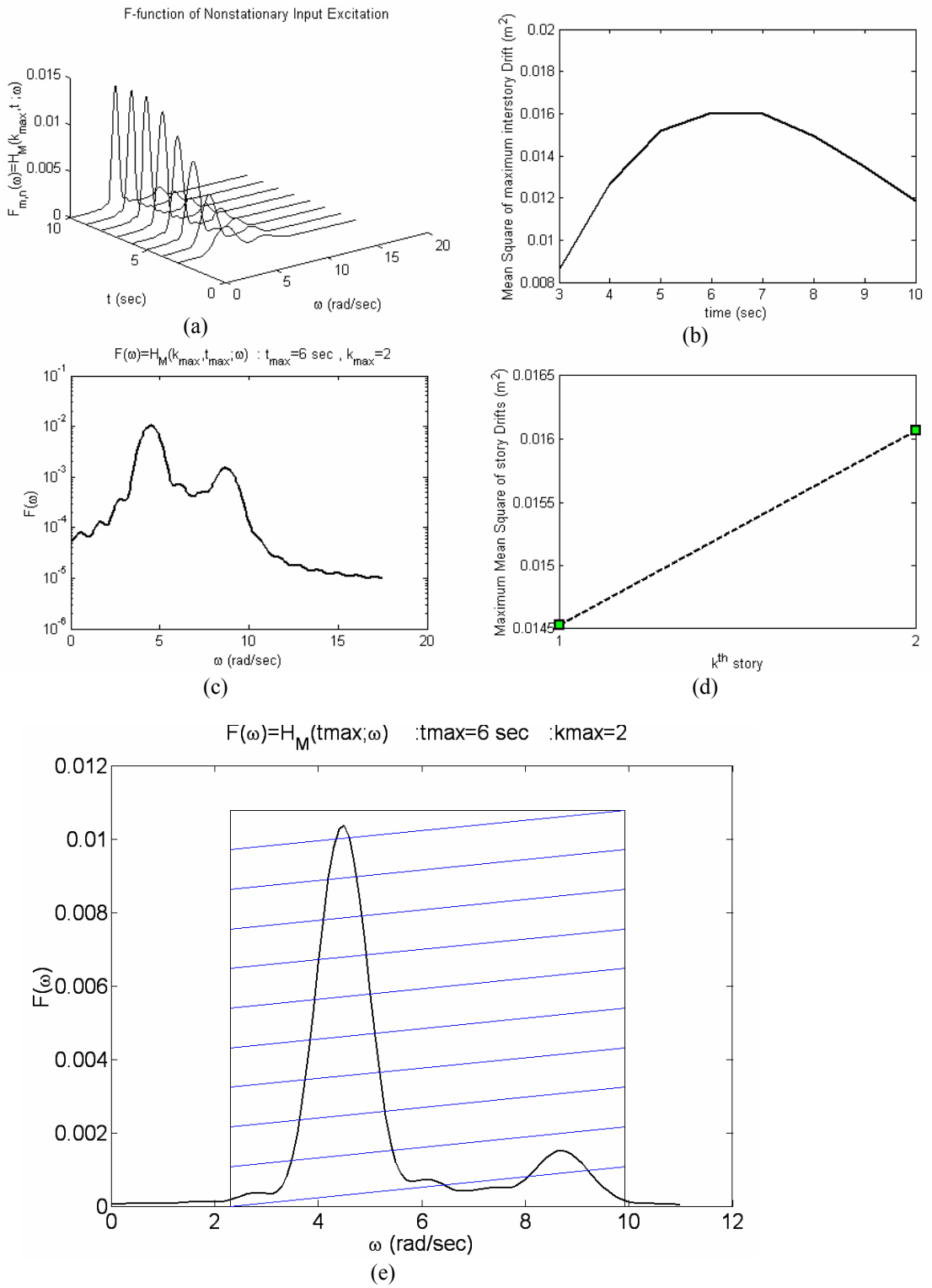

Fig. 13. Non-stationary critical excitation for Model 1 under Tabas (1978) constraints

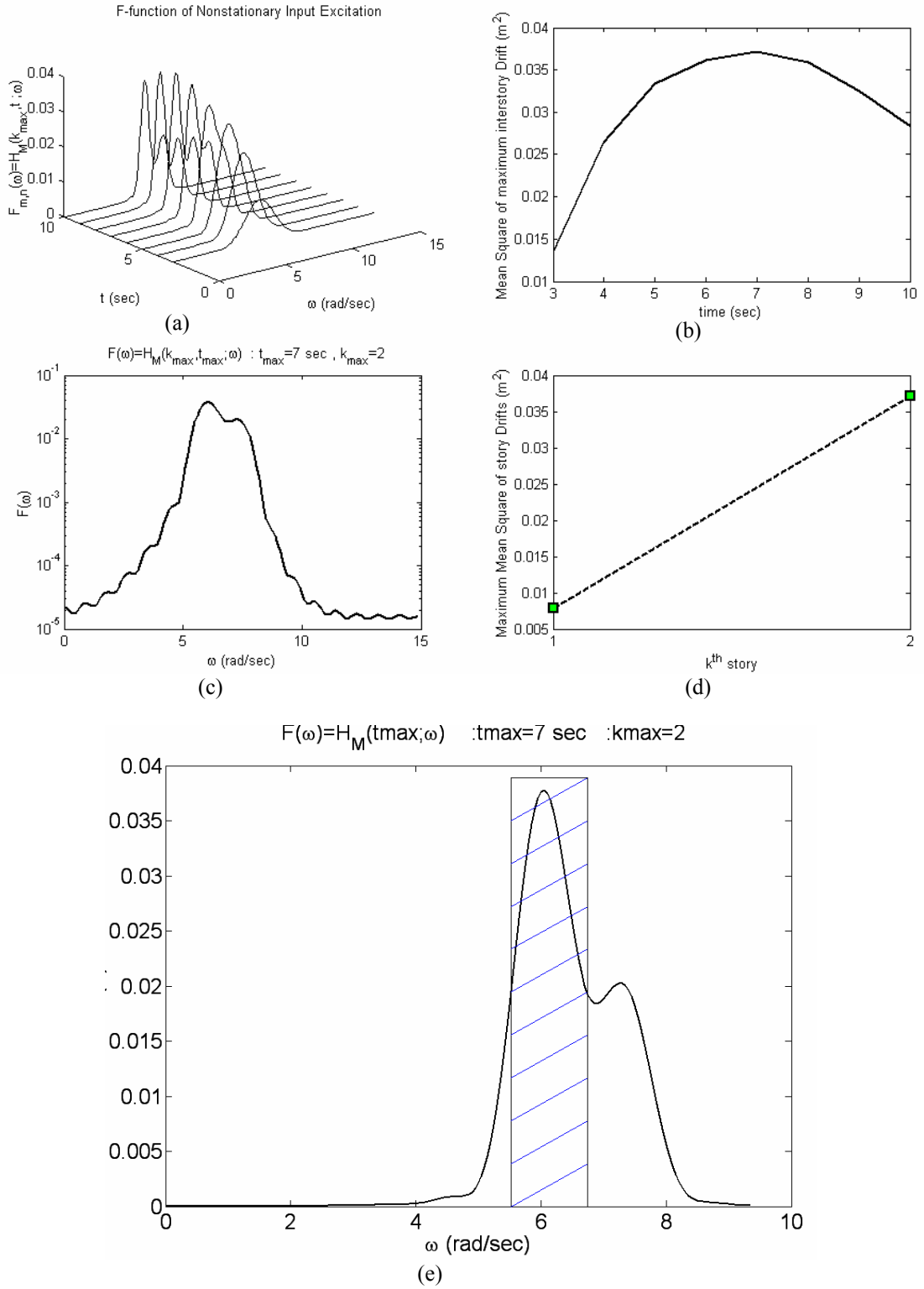

Fig. 14. Non-stationary critical excitation for Model 2 under El-Centro constraints (NS 1940): $\delta\omega = 0.2$

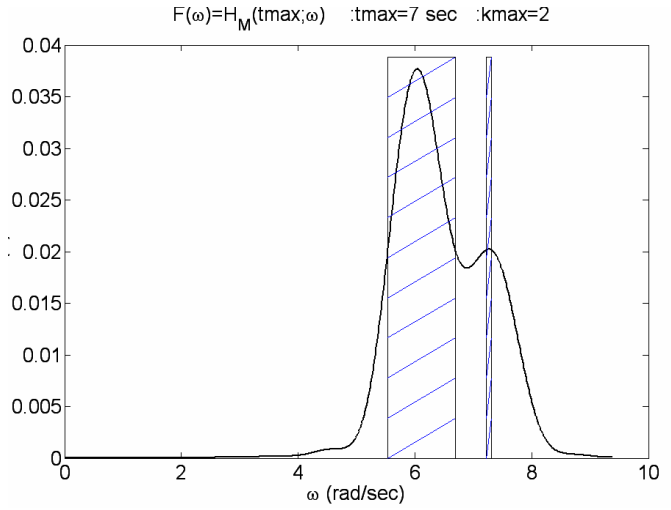

Fig. 15. Non-stationary critical excitation for Model 3 under El-Centro constraints (NS 1940): $\delta\omega = 0.04$

Table 1. Numerically optimized critical excitation of Model 2 for El-Centro (NS 1940)

Model 2, $\xi = 0.05$ El-Centro (NS 1940)		$\delta\omega(rad/\sec) =$		
		0.50	*0.20*	*0.01*
Simple technique of optimization	$\omega_{1start} - \omega_{1end} =$	*5.50-6.50*	*5.6-6.80*	*5.54-6.69*
	$\omega_{2start} - \omega_{2end} =$	--------	--------	*7.23-7.31*
	$Max(f) =$	3.6331×10^{-2}	3.6619×10^{-2}	3.6803×10^{-2}
Modified technique of optimization	$\omega_{1start} - \omega_{1end} =$	*5.5213-6.7535*	*5.5127-6.7417*	*5.5375-6.6917*
	$\omega_{2start} - \omega_{2end} =$	--------	---------	*7.2285-7.3064*
	$Max(f) =$	3.6921×10^{-2}	3.67148×10^{-2}	3.6815×10^{-2}

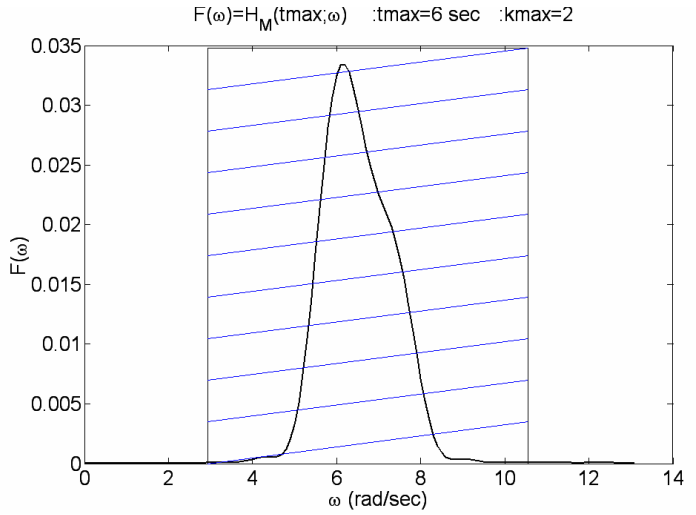

Fig. 16. Non-stationary critical excitation for Model 2 under Tabas (1978) constraints

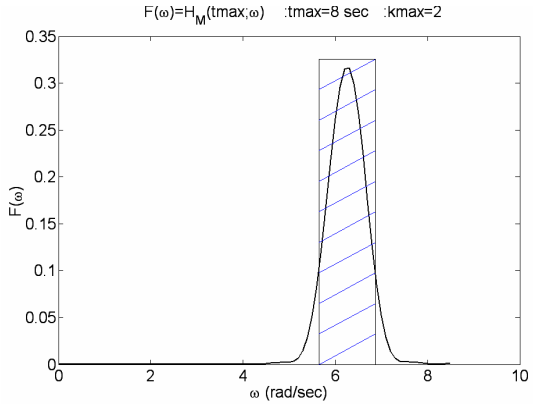

Fig. 17. Non-stationary critical excitation for Model 3 under El-Centro constraints (NS 1940)

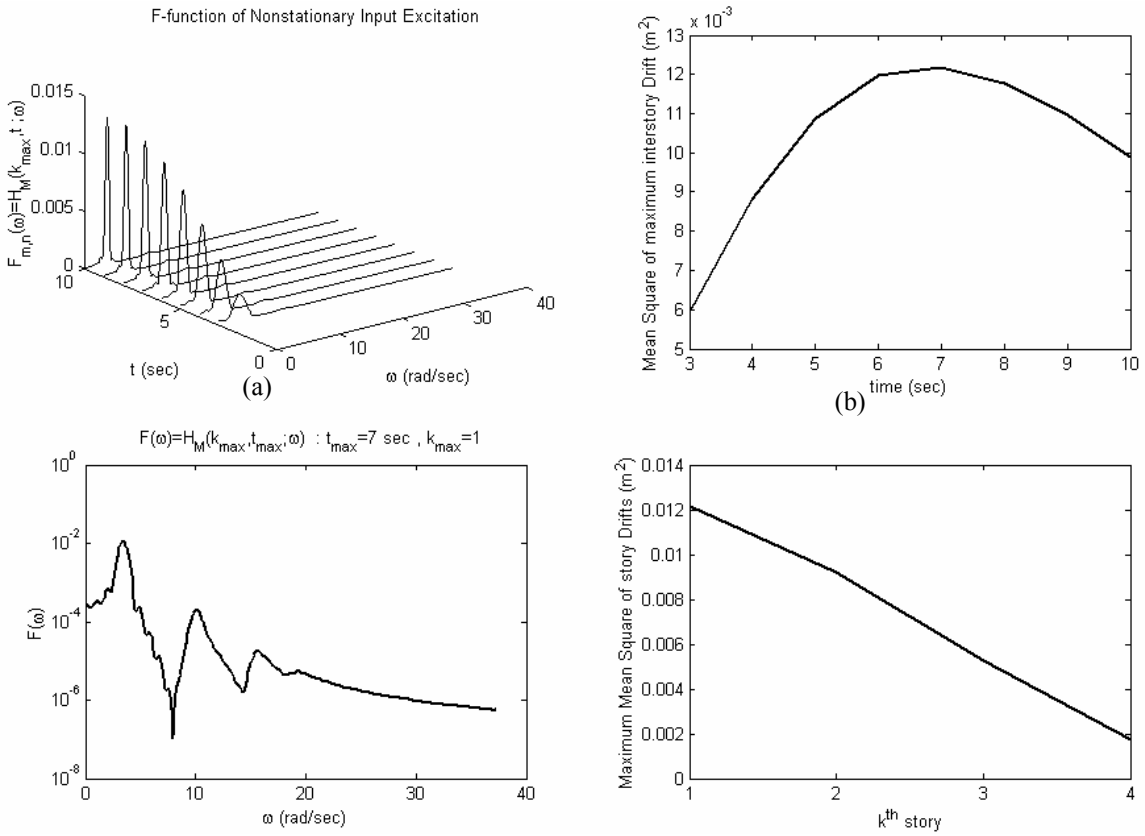

Fig. 18. Non-stationary critical excitation for 4-story model under Tabas (1978) constraints

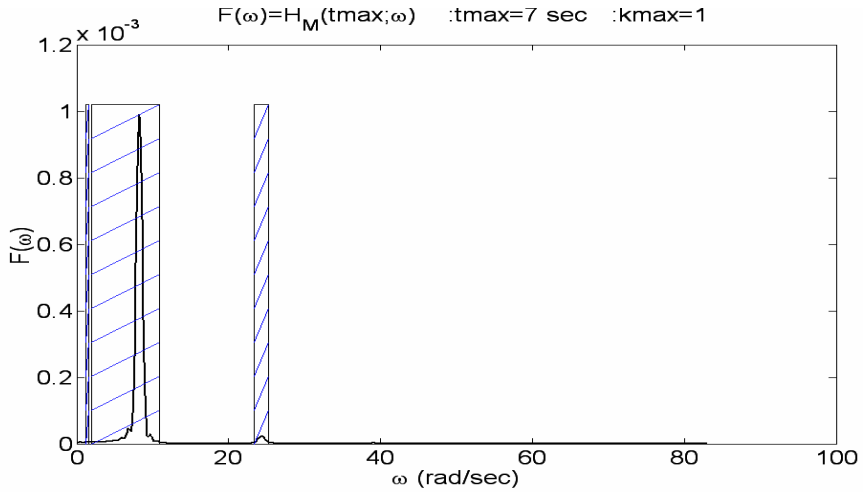

Fig. 19. Non-stationary critical excitation for 6-story model under H-N constraint (JMA Kobe NS 1995)

5. CONCLUSION

The results can be summarized as follows:

1) A new non-stationary critical excitation optimization problem has been proposed having a new and better objective function that states the real damage of a structure. In the proposed objective function, the mean square of the inter-story drifts is maximized at different times and stories.
2) A new modified technique of solving non-stationary critical excitation optimization problem has been proposed for MDOF systems to compute more exact results in fewer numbers of steps and shorter time.
3) The shape of the frequency response F-function has been investigated for different modal frequency adjacency cases. It is observed that for non-stationary cases, F-function has many small peaks and its principle peaks may combine.
4) The proposed technique presents the critical input excitation as the rectangular frequency bandwidths around the natural modal frequencies to resonate the model. Maximum number of these rectangular frequencies is equal to the degrees of freedom of the system. For narrow bandwidth inputs, critical excitation becomes only one rectangular frequency around the first mode. For wideband inputs, frequency bandwidth around the frequencies of the high modes will participate in critical input excitation to cause resonance response of higher modes of structure with input excitation. Therefore, it is obvious that the first mode is more important for the resonance of structural vibration with input excitation.

Acknowledgement- The authors would like to thank Mr. S.R. Massah for revising some parts of the paper.

REFERENCES

1. Papoulis, A. (1967). Limits on band limited signals. *Proceedings of IEEE*, Vol. 55, 10, pp. 1677-1686.
2. Drenick, R. F. (1970). Model-free design of aseismic structures. *Journal of Engineering Mechanics Division ASCE*, Vol. 96, No. EM4, pp. 483-493.
3. Shinozuka, M. (1970). Maximum structural response to seismic excitations. *Journal of Engineering Mechanics Division ASCE*, Vol. 96, No. EM5, pp. 729-738.
4. Iyengar, R. N. (1972). Worst inputs and a bound on the highest peak statistics of a class of non-linear systems. *Journal of Sound and Vibration*, Vol. 25, pp. 29-37.

5. Iyengar, R. N. & Manohar, C. S. (1987). Non-stationary random critical seismic excitations. *Journal of Engineering Mechanics, ASCE*, Vol. 113, No. 4, pp. 529-541.
6. Manohar, C. S. & Sarkar, A. (1995). Critical earthquake input power spectral density function models for engineering structures. *Earthquake Engineering and Structural Dynamics*, Vol. 24, pp. 1549-1566.
7. Sarkar, A. & Manohar, C. S. (1998). Critical seismic vector random excitations for multiply supported structures. *Journal of Sound and Vibration*, Vol. 212, No. 3, pp. 525-546.
8. Takewaki, I. (2001). A new method for non-stationary random critical excitation. *Earthquake Engineering and Structural Dynamics*, Vol. 30, pp. 519-535.
9. Takewaki, I. (2002). Robust building stiffness design for variable critical excitations. *Journal of Structural Engineering*, Vol. 128, No. 12, pp. 1565-1574.
10. Ben-Haim, Y. & Elishakoff, I. (1990). *Convex models of uncertainty in applied mechanics.* Elsevier: Amsterdam.
11. Pantelides, C. P. & Tzan, S. R. (1996). Convex model for seismic design of structures: I analysis. *Earthquake Engineering and Structural dynamic*. Vol. 25, pp. 927-944.
12. Ghodrati, G., Ashtari, P. & Rahami, H. (2006). New development of artificial record generation by wavelet theory. *International Journal of Structural Engineering and Mechanics*, Vol. 22, No. 2, pp. 185-195.
13. MacCann, W. M. & Shah, H. C. (1979). Determining strong-motion duration of earthquake. *Bulletin of the Seismological Society of America*, Vol. 69, pp. 1253-1265.
14. Ashtari, P. (2006). *Seismic design and evaluation of structures using critical excitation method*. Doctoral dissertation, College of Civil Engineering, Iran University of Science & Technology, Tehran, Iran.
15. Ghodrati, G. & Ashtari, P. (2004). Optimization technique for finding probabilistic critical excitation. *Proceedings of 7th International Conference on Probabilistic Safety Assessment and Management PSAM7*, Berlin.
16. Ghodrati, G. & Ashtari, P. (2004). Optimal critical response of multi-story buildings to random input excitations. *Proceeding of 13th World Conference on Earthquake Engineering*, Vancouver, B.C. Canada.
17. Bendat, J. S. & Piersol, A. G. (1986). *Random data: analysis and measurement procedures*. John Wiley & Sons, Inc.
18. Craig, R. R. (1982). *Structural dynamics*. John Wiley & Sons: New York.
19. Bikce, M., Aksogan, O. & Arslan, H. M. (2004). Stiffened multi-bay coupled shear walls on elastic foundation. *Iranian Journal of Science & Technology, Transaction B, Engineering*, Vol. 28, No. B1, pp. 43-52.